Phase decomposition study in $Co_xFe_{3-x}O_4$ iron cobaltites: Synthesis and structural characterization of the spinodal transformation

H. Le Trong, A. Barnabé*, L. Presmanes, Ph. Tailhades

Institut Carnot CIRIMAT – UMR CNRS 5085, Université Paul Sabatier Toulouse III, 118 Route de Narbonne, 31062 Toulouse Cedex 4, France

Abstract

$Co_xFe_{3-x}O_4$ iron cobaltites ($1.21 < x < 2.35$) have been prepared in the form of submicronic particles from mixed oxalic precursors heat treated at 900 and 600 °C. The samples obtained at 900 °C are made of a single spinel phase in which Co^{2+} and Fe^{3+} ions are distributed in both octahedral and tetrahedral sites and Co^{3+} ions are only located in the octahedral sublattice. For heat treatments carried out at 600 °C two spinel phases are formed according to the phase diagrams. Pure $Co_{1.7}Fe_{1.3}O_4$ oxide annealed at 700 °C progressively transformed into two iron-rich and cobalt-rich spinel phases, respectively. More than 120 h of heat treatment is required to get the complete decomposition of the pristine oxide. At the beginning this oxide is submitted to a spinodal transformation. Alternating regions of iron-rich and cobalt-rich spinels are then created. The periodicity of the nanostructuration of the material is estimated to be close to 5 nm.

Keywords: Spinel; Iron cobaltites; Cobalt ferrites; Spinodal decomposition; Self-organization

1. Introduction

Many researchers are working on artificially organized magnetic materials with the aim to prepare magnetic devices (magnetic tunneling junction, spin valves, spin filters, magnonic or magneto-photonic crystals) [1–5]. They have succeeded in building these organizations at the submicrometric scale using thin film deposition methods, such as pulsed laser deposition, sputtering or molecular beam epitaxy, which are sometimes associated to photolithographic processes.

In other scientific fields, some authors are trying to prepare organized materials taking the benefit of pure or assisted self-organization phenomena of small monodispersed particles [6–9]. 2D or 3D periodic assemblies of micronic or nanometric spheres can be prepared by this manner. Interesting collective properties result from such periodic layouts. For instance, ''super-crystals'' made of small monodispersed particles of silica can display photonic band gap properties [10]. Magnetic 2D or 3D self-organized particles, thin films or bulk materials, are also very attractive because they can display giant magnetoresistance (GMR) and tunneling magnetoresistance (TMR) properties.

For magnetic thin films or bulk materials, self-organization can be induced by spontaneous crystalline transformations [11–13] but among them, the spinodal decomposition seems to be the most suitable. The spinodal decomposition is a phase segregation mechanism, which can occur in a miscibility gap of a phase diagram. This out of equilibrium process leads to pseudo-periodic distribution of the precipitated phases when interrupted before end. Materials with alternate nanometric layers of two different phases can then be created. Because of their organization which is similar to the artificially prepared GMR multilayered films [1], some of them display the GMR property. This was observed in some ferromagnetic alloys [11–13].

This work is focused on $Co_xFe_{3-x}O_4$ mixed cobalt iron oxides, especially on the $Co_{1.7}Fe_{1.3}O_4$ oxides which have a chemical composition within the miscibility gap of the

* Corresponding author. Tel.: +33 5 61 55 77 51; fax: +33 5 61 55 61 63.
E-mail address: barnabe@chimie.ups-tlse.fr (A. Barnabé).

doi:10.1016/j.solidstatesciences.2007.10.004

Fe_3O_4–Co_3O_4 phase diagram [14–18]. Spinel iron cobaltites with x in between 0.5 and 1.5 can be submitted to spinodal decomposition when heat treated for several hours at about 500–700 °C [16,17]. The stacking-up of alternate nanometric layers of cobalt-rich and iron-rich spinel phases was then observed in the material. The purpose of our study is to characterize the cationic distribution of the spinel phases formed inside the miscibility gap of the Fe_3O_4–Co_3O_4 phase diagram on one hand, and to specify the preparation conditions required to obtain the best-suited periodic structures to get new GMR materials in the future, on the other hand.

2. Experimental procedures

Spinel iron cobaltites were synthesized according to the previously described *chimie douce* method using oxalate precursors $(Co_xFe_{3-x})_{1/3}C_2O_4{,}2H_2O$ [19]. A concentrated solution of cobaltous and ferrous chlorides was reacted with an oxalic acid solution to get a precipitate of oxalates. Iron(II) chloride hydrate $FeCl_2 \cdot 4H_2O$ and cobalt(II) chloride hydrate $CoCl_2 \cdot 6H_2O$ were weighted in the appropriate Co/Fe molar ratio. The metallic salts were initially dissolved in a mixture of water, ethylene glycol, and hydrochloric acid, while the oxalic acid was dissolved in an ethyl alcohol (95%) and water (5%) mixture.

After drying, grinding and sieving, the oxalate powders were decomposed in air at different temperatures from 600 to 900 °C to get iron cobaltites.

The morphology of the powders was determined by scanning electron microscopy (SEM) using a Jeol JSM 6400 electron microscope. To check the purity of these phases and to measure the lattice constants, all samples were analyzed by X-ray diffraction (XRD) using a Bruker D4 Endeavor X-ray diffractometer. XRD patterns were refined by the Rietveld method implanted in the FullProf/WinPlotR software package [20]. Thermogravimetric measurements (TG) were carried out in air with a Setaram TG 92 apparatus. Magnetic properties were measured by a S2IS M2000 pulsed-field magnetometer, which allows the application of a maximum magnetic field of 25 kOe. The measurements were done at room temperature on packed samples (packing density close to 0.5 g/cm^3). The Co and Fe contents were estimated by plasma emission spectroscopy.

The Electron Diffraction (ED) and High Resolution Electron Microscopy (HREM) studies were carried out using a Jeol TEM-FEG 2100F electron microscope operating at 200 kV and equipped with an X-EDS analyzer.

3. Results and discussion

3.1. Oxalate powders

The oxalate powders are made of elongated particles, as it was already revealed for different transition metal oxalates prepared by similar experimental conditions [21,22]. The size and the shape of the particles remain approximately the same when the cobalt content x varies from 1.21 to 2.35. As an example, the FEG-SEM micrograph of cobalt iron oxalate $(Co_xFe_{3-x})_{1/3}C_2O_4{,}2H_2O$ with $x = 1.48$ is shown in Fig. 1. The XRD patterns were indexed using the crystallographic data for the β-form of the dihydrate iron oxalate according to the monoclinic humboldtine structure type (PDF card # 23-0293). No extra phase was detected. The lattice constant and the unit cell volume evolved according to cobalt content, in between the corresponding parameters for pure iron and cobalt oxalates (Table 1 and Fig. 2). Crystallite's average size determined by the Scherrer' law is close to 100 nm in accordance with the SEM images. TG measurements were carried out on the Co–Fe oxalic precursors on one hand, and on both pure iron and cobalt oxalates and on their mixtures on the other. TG curves show undoubtedly that their thermal behavior is characteristic of homogeneous and single phased oxalate (Fig. 3). The TG curves for Co–Fe oxalates display halfway shapes between pure cobalt and iron oxalate thermograms, which are completely different from the TG of their mixture.

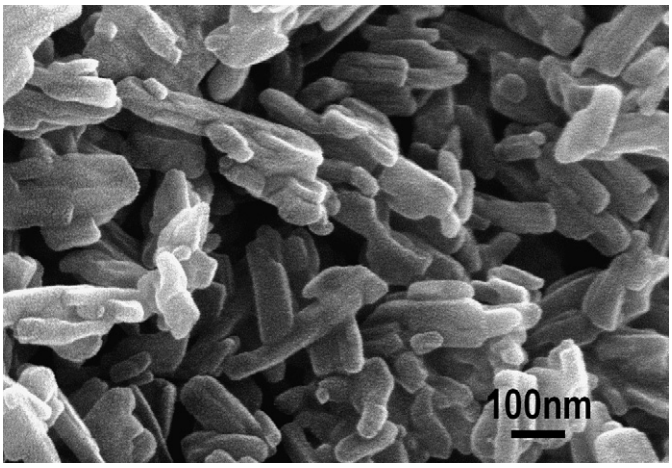

Fig. 1. FEG-SEM micrograph of cobalt iron oxalate $(Co_xFe_{3-x})_{1/3}C_2O_4{,}2H_2O$ with $x = 1.48$.

3.2. Oxide powders prepared from oxalate decomposition at 900 and 600 °C

The oxalate powders decomposed at 900 °C and then quenched in air to room temperature are made of a single spinel oxide phase, whatever the cobalt content is. When decomposed at 600 °C the powders are single phased only for x lower than 1.2 and for x higher than 2.4. In between these two cobalt

Table 1
Refined lattice parameters of cobalt iron oxalate $(Co_xFe_{3-x})_{1/3}C_2O_4{,}2H_2O$ with $1.21 \leq x \leq 3.00$ according to the β-form of the dihydrate iron oxalate (humboldtine: space group *I2/a*, PDF # 23-0293)

$(Co_xFe_{3-x})_{1/3}C_2O_4{,}2H_2O$	a (Å)	b (Å)	c (Å)	γ (°)
$x = 1.21$	9.885(3)	5.493(1)	9.814(2)	104.07(1)
$x = 1.48$	9.876(2)	5.485(1)	9.811(2)	104.28(1)
$x = 1.69$	9.852(1)	5.472(1)	9.814(2)	104.38(1)
$x = 1.94$	9.850(1)	5.463(1)	9.825(1)	104.48(1)
$x = 2.14$	9.857(2)	5.454(1)	9.824(2)	104.66(1)
$x = 2.35$	9.820(2)	5.442(1)	9.843(1)	104.82(1)
$x = 3.00$	9.787(2)	5.421(1)	9.852(1)	105.10(1)

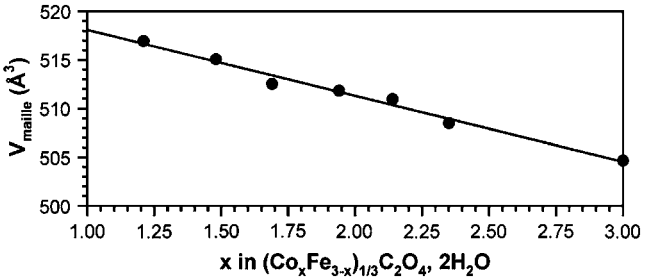

Fig. 2. Unit cell volume of cobalt iron oxalate $(Co_xFe_{3-x})_{1/3}C_2O_4{,}2H_2O$ with $1.21 \leq x \leq 3.00$.

contents, the powders are made of two spinel phases according to the miscibility gap of the Fe_3O_4–Co_3O_4 system, previously revealed by the experimental [14–17] or calculated [18] phase diagrams, already published by several authors.

For x in between 1 and 2, several authors [23–25] have proposed structural formulas in agreement with the general cationic distribution:

$$Fe^{3+}_{1-\alpha}Co^{2+}_{\alpha}\left[Fe^{3+}_{2-x-\alpha}Co^{2+}_{1-\alpha}Co^{3+}_{x-1}\right]O^{2-}_4 \quad (1 \leq x \leq 2, \alpha \leq 1) \qquad (1)$$

in which α varies with the cobalt content from about 0.5 to 0.8, for the range of composition studied for the present work. According to this assumption, tetrahedral Co^{3+} ions are not taken into account because of the strong octahedral preference of these ions. Using the same approach, a cationic distribution can be proposed when x is higher than 2 and lower than 3. It can be expressed by the following formula:

$$Fe^{3+}_{3-x-\omega}Co^{2+}_{x-2+\omega}\left[Fe^{3+}_{\omega}Co^{2+}_{3-x-\omega}Co^{3+}_{x-1}\right]O^{2-}_4 \quad (2 \leq x \leq 3,\ \omega \leq 3-x) \qquad (2)$$

The lattice constants of the spinel cobaltites obtained at 900 °C decrease with the cobalt content (Fig. 4). According

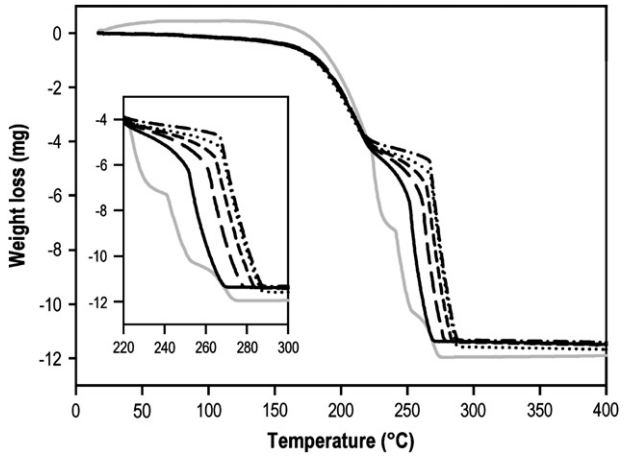

Fig. 3. DTG and DTA curves in air (heating rate = 10 °C/min) of cobalt iron oxalate $(Co_xFe_{3-x})_{1/3}C_2O_4{,}2H_2O$ with $x = 1.21$ (solid), $x = 1.48$ (long dash), $x = 1.69$ (short dash), $x = 1.94$ (dotted) and $x = 2.14$ (dash-dot). DTA and TGA of a mechanical mix of cobaltous and ferrous oxalates in the $x = 1.70$ ratio is represented in grey solid line.

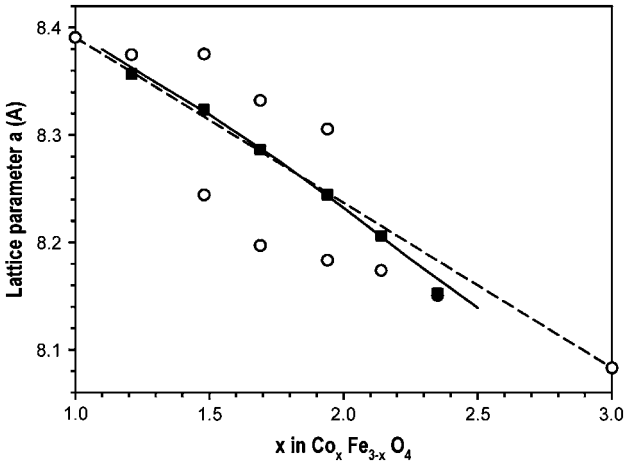

Fig. 4. Lattice parameter of cobalt iron oxide $Co_xFe_{3-x}O_4$ with $1.21 \leq x \leq 3.00$ according to the cubic spinel form (space group $Fm\bar{3}m$, no 227) for $T = 600$ °C (white circle) and $T = 900$ °C (black square). The evolution of the lattice parameter according to the Vegard's law in between $CoFe_2O_4$ (PDF # 22-1086 with $a = 8.3910$ Å) and Co_3O_4 (PDF # 41-1467 with $a = 8.083$ Å) is represented in dash line. The solid line corresponds to the lattice parameter calculated by the Poix's equation according to the (1) and (2) cation distribution.

to Poix [26], the lattice constant a of the spinel phases can be calculated from:

$$a = 2.0995d_{Td} + \left[5.8182\left(\frac{d_{Oh}}{2}\right)^2 - 1.4107d_{Td}^2\right]^{1/2} \qquad (3)$$

whereas d_{Td} and d_{Oh} are the mean average cation–oxygen distances in tetrahedral and octahedral sites, respectively (Table 2). In agreement with the bibliographical data, a good fit of the $a = f(x)$ curve can be obtained when the quantity of tetrahedral Co^{2+} ions (equal to α, when $1 \leq x \leq 2$ and equals to $x - 2 + \omega$, when $2 \leq x \leq 2.5$) is close to $(-x^2 + 3.6x - 2.5)$ (Fig. 4). That means the quantity of cobalt ions in tetrahedral sites lies from about 0.25 to 0.75.

The $Co_xFe_{3-x}O_4$ oxides with $1.2 < x < 2.4$ resulting from heat treatments at 600 °C for half an hour are made of iron-rich and cobalt-rich spinel phases, which display high and low lattice constants, respectively (Fig. 4). Due to the shape of the miscibility gap in the phase diagram [17], the unit cells of these phases would have to be the same. The differences between the measured lattice constants reveal that the thermodynamic equilibrium state is not reached for the experimental conditions. We have then chosen to study more carefully the formation of the iron-rich and cobalt-rich phases when x is

Table 2
Average cation–oxygen distances in tetrahedral (d_{Td}) and octahedral (d_{Oh}) sites used for the $Co_xFe_{3-x}O_4$ lattice parameter calculation according to the Poix's formulae [26]

d(M–O) bond lengths (Å)	Fe^{III}	Co^{II}	Co^{III}
In tetrahedral site (Td)	1.858	1.974	–
In octahedral site (Oh)	2.020	2.123	1.892

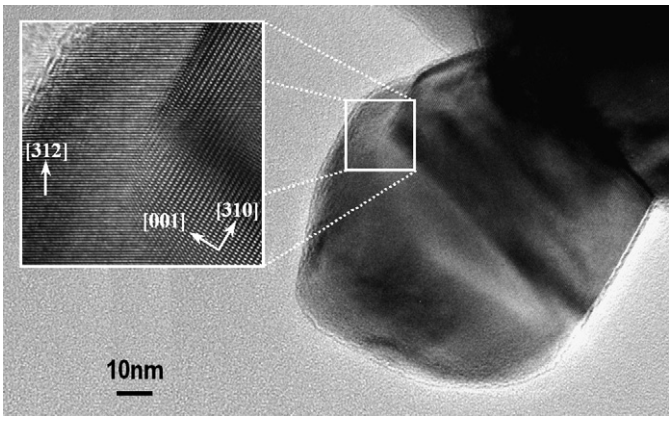

Fig. 5. TEM micrograph for a sample prepared at 900 °C with a homogeneous 0.56 Co/Fe ratio and without any Moiré fringe. Inset is the HRTEM micrograph showing oriented domains within the grain.

equal to 1.7. This composition, close to the median part of the miscibility gap, is interesting because it can be subjected to spinodal decomposition [17].

3.3. Annealing at 700 °C of $Co_{1.7}Fe_{1.3}O_4$ powders prepared at 900 °C

The $Co_{1.7}Fe_{1.3}O_4$ sample prepared at 900 °C exhibits in the XRD pattern a single spinel phase with $a = 8.2862$ Å corresponding to the composition $x = 1.70$. TEM and X-EDS analysis indicate homogeneous characteristics with an average crystallites size close to 100 nm and with a constant Co/Fe ratio equal to 0.56 (or $x = 1.70$ in the $Co_xFe_{3-x}O_4$ formulae). No significant variation is detected from the whole grain X-EDS analysis and local analysis made with an electron probe close to 1 nm in STEM mode. An example of the typical microstructure seen in this sample is shown in Fig. 5. Well organized oriented domains are present in the whole crystal. Inset zoom in Fig. 5 shows oriented domains with exactly the same chemical composition.

This pristine phase was then annealed at 700 °C for different durations. Along this annealing, the starting spinel phase is decomposed into two other phases according to the phase diagram. The kinetic of the transformation is very slow as illustrated by the $a = f(\text{time})$ curves for each phase (Fig. 6a). More than 120 h of treatment is required to reach the complete decomposition of the starting spinel oxide and to get two other spinel phases, with lattice constants stabilized at the ultimate values of $a = 8.372$ Å and $a = 8.130$ Å. These lattice constants are characteristics of Co−Fe spinel phases having compositions close to $Co_{1.1}Fe_{1.9}O_4$ and $Co_{2.7}Fe_{0.3?}O_4$, respectively. Fig. 6b shows the development of the 311 Bragg reflection of the cubic spinel phase in samples annealed at $T = 700$ °C for different durations. The peak profile of samples annealed for intermediate time shows a central peak which corresponds to the position of the 311 Bragg reflection of the starting spinel phase ($x = 1.70$). On top of that, a second set of peaks appear on the low-angle side and on the high-angle side, corresponding to the Fe-rich phase and the Co-rich phase, respectively. At the end of the decomposition, the phases then display cobalt rates in agreement with the phase diagram reported by Hirano et al. [17].

For intermediate annealing time, X-EDS analysis of the whole crystallite indicates that the Co/Fe average ratio is still equal to 0.56 ($x = 1.70$). Fluctuations in chemical composition are observed from place to place inside the crystal when the electron probe is reduced close to 1 nm: three domains can be observed in accordance with the Co/Fe ratio of the pristine phase ($x = 1.70$), with the Co-rich phase ($x = 2.7$) and Fe-rich phase ($x = 1.6$). The typical microstructure in this sample is obscured by sets of Moiré fringes which occur throughout the specimen as shown in Fig. 7 for the 36 h annealed sample. Moiré fringes are always located in between the pristine phase and the Co- or Fe-rich phase determined by X-EDS analysis. They are characteristic of the spinodal decomposition [27].

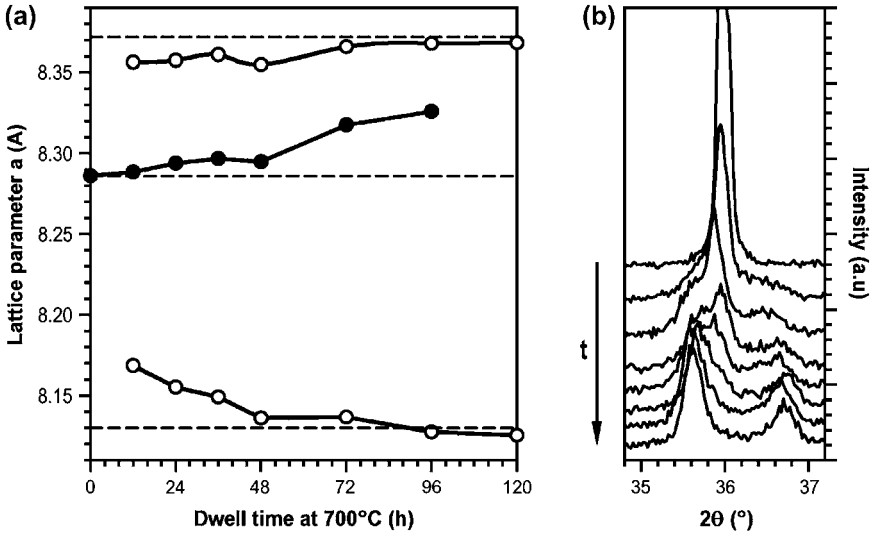

Fig. 6. Plot of the lattice parameter versus time (a) and corresponding 311 Bragg reflection (b) for sample prepared at 900 °C and annealed at 700 °C for different times.

They are a consequence of double diffraction from two overlapping phases which either have slightly different lattice spacing or are slightly rotated with respect to each other [28]. The microstructure observed in this kind of zone consists of fine-scale modulations as shown in Fig. 8 for the 36 h annealed sample. The wavelength of the modulation is estimated to be around 5 nm. The corresponding Fourier function transform of this area confirms the superposition of cubic spinel reciprocal lattices slightly rotated with respect to each other (Fig. 8).

When the sample is treated for more than 48 h at 700 °C, Moiré fringes and then periodic structures tend to vanish. For the 120 h annealed sample, the pristine spinel phase cannot be detected anymore in the XRD pattern (Fig. 6) and the Moiré fringes are no more observed in TEM micrographs. Crystallites exhibit well organized chemical Co-rich and Fe-rich domains with clean grain boundaries (Fig. 9).

3.4. $Co_{1.7}Fe_{1.3}O_4$ oxides directly prepared from oxalate decomposition at 700 °C

Oxides containing the same cobalt content as previously were directly prepared by oxalate decomposition at 700 °C. They were kept at this temperature for different durations and then quenched in air to room temperature. The oxalate decomposition led to the formation of only two spinel oxides with lattice parameters consistent with a Co-rich and Fe-rich phases. No intermediate spinel phase with lattice parameter close to 8.28 Å could be detected, showing that the spinodal transformation did not occur. The curves of lattice constants versus time and development of the 311 Bragg reflection of the spinel phases are plotted in Fig. 10. The upper curve is ascribed to the iron-rich phase because the substitution of cobalt ions to iron ions tends to increase the lattice constant. No significant change seems to occur for this phase along the heat

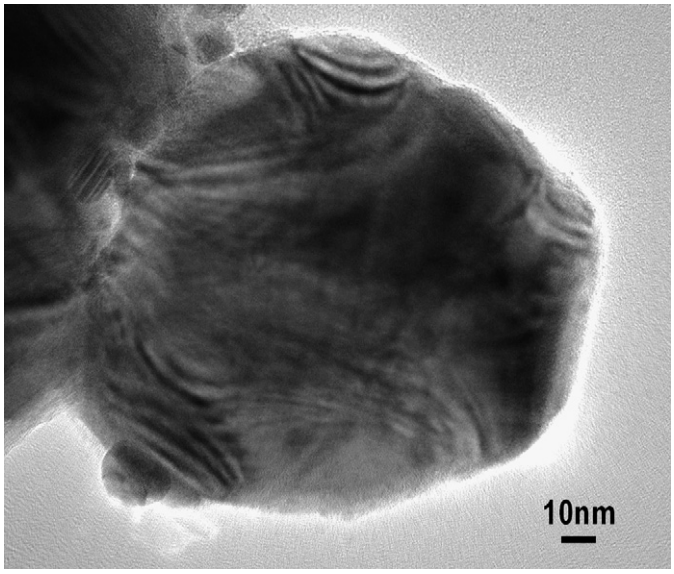

Fig. 7. TEM micrographs of samples prepared at 900 °C and annealed 36 h at 700 °C showing Moiré fringes in different places within the crystal.

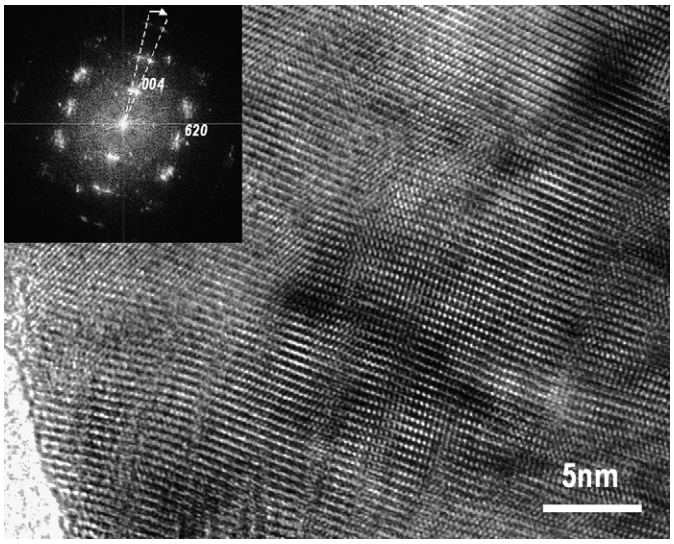

Fig. 8. HRTEM micrograph of sample prepared at 900 °C and annealed 36 h at 700 °C showing the fine-scale modulations of the two spinel phases due to spinodal transformation. Inset is the corresponding Fourier function transform of the modulated area showing the superposition of cubic spinel reciprocal lattices slightly rotated with respect to each other.

treatment, because the unit cell does not vary. However, the unit cell of the cobalt-rich phase evolves according to the upholding time at 700 °C. A drastic drop of the lattice constant is observed for the first 24 h of the treatments. This drop, close to 0.0045 Å, is too large to be only explained by migration of cations from one sublattice to another in the same spinel structure. For instance, the lattice constant calculated for $Co_{2.5}Fe_{0.5}O_4$ decreases for less than 0.0016 Å, when the spinel goes from normal to statistically disordered cationic distribution.

The impoverishment in iron of the cobalt-rich phase to the iron-rich spinel seems to be the most probable mechanism to explain the decrease in lattice constant. This assumption is supported by the increase in saturation magnetization at

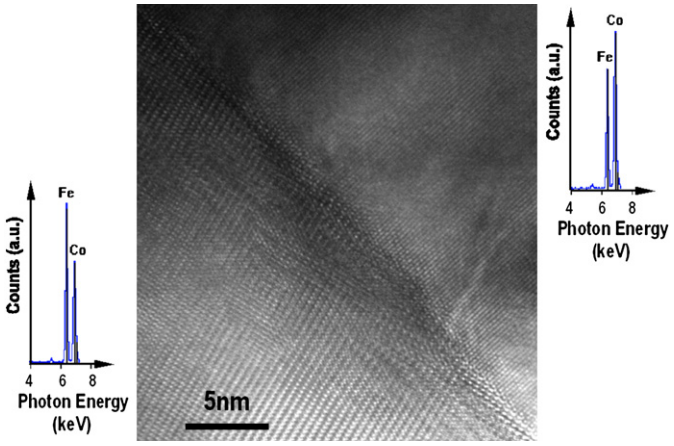

Fig. 9. HREM micrograph of sample prepared at 900 °C and annealed 120 h at 700 °C showing well defined grain boundaries in between two crystals with different chemical compositions. Inset is the corresponding X-EDS local analysis spectra.

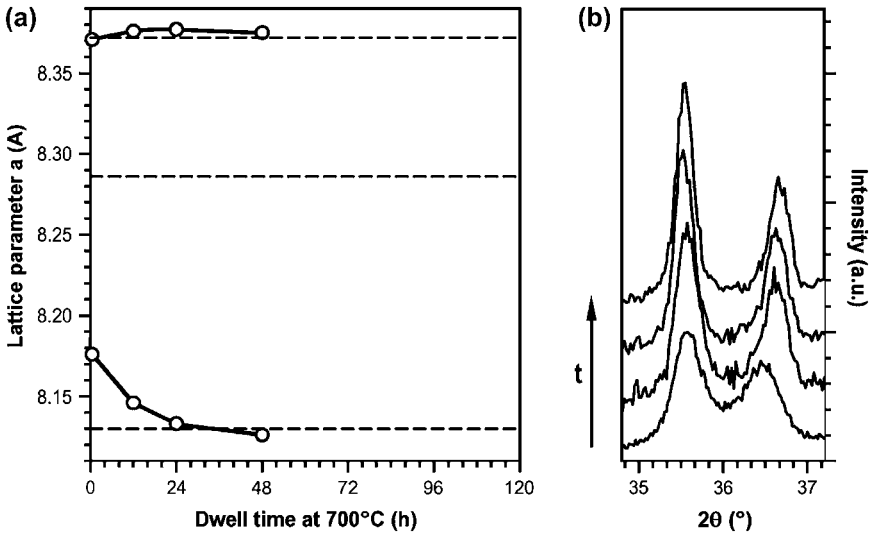

Fig. 10. Plot of the lattice parameter versus time (a) and corresponding 311 Bragg reflection (b) for sample prepared at 700 °C and annealed at 700 °C for different times.

room temperature versus the heat treatment duration (Fig. 11). In fact, the Curie temperatures of $Co_xFe_{3-x}O_4$ spinels are lower than room temperature, when x is higher than about 2.5 [17]. For the samples prepared at 700 °C, the ferrimagnetic properties at room temperature are then exclusively due to the iron-rich phase contribution and the increase in saturation magnetization can be ascribed to a higher content of the ferrimagnetic iron-rich phase.

Similar behavior is observed when the phases are formed at 600 °C. When heat treated for longer time, the phase lattice constant tends to reach the previously observed values for the treatments at 700 °C. The kinetic is very low: after 144 h at 600 °C the cobalt-rich spinel still does not reach the same lattice constant as that of the sample treated at 700 °C for 48 h.

4. Conclusions

$Co_xFe_{3-x}O_4$ iron cobaltites ($1.21 < x < 2.35$) have been prepared in the form of submicronic particles from mixed oxalic precursors heat treated at 900 and 600 °C. The samples obtained at 900 °C are made of a single spinel phase which can be described by the structural formula $Fe^{3+}_{1-\alpha}Co^{2+}_{\alpha}[Fe^{3+}_{2-x-\alpha}Co^{2+}_{1-\alpha}Co^{3+}_{x-1}]O^{2-}_4$ ($\alpha \leq 1$) when x is lower than 2 or $Fe^{3+}_{3-x-\omega}Co^{2+}_{x-2+\omega}[Fe^{3+}_{\omega}Co^{2+}_{3-x-\omega}Co^{3+}_{x-1}]O^{2-}_4(\omega \leq 3-x)$ when x is higher than 2. The tetrahedral cobalt ions' content lies from 0.25 to 0.75. For heat treatments carried out at 600 °C two spinel phases are formed according to the phase diagrams already published.

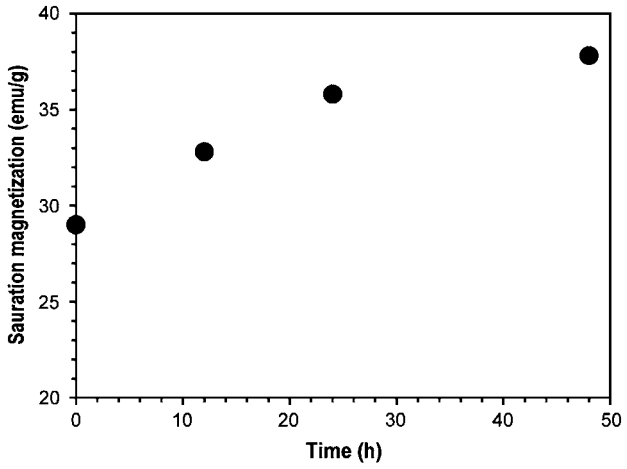

Fig. 11. Plot of the saturation magnetization registered at room temperature versus the heat treatment duration for samples prepared at 700 °C.

Pure $Co_{1.7}Fe_{1.3}O_4$ oxide annealed at 700 °C is progressively transformed into two iron-rich and cobalt-rich spinel phases, respectively. The kinetic of the phase transformation is very slow. More than 120 h of heat treatment were required to get the complete decomposition of the pristine oxide. At the beginning the oxide is submitted to a spinodal transformation as revealed by Moiré fringes in transmission electron micrographs. Alternating regions of iron-rich and cobalt-rich spinels are then created. Their periodicity is estimated to be close to 5 nm.

Further investigations have to be performed now, with the aim of revealing specific properties related to the periodic organization at the nanometric scale of these materials.

Acknowledgment

Le Trong Hoa thanks the Vietnam Ministry of Education and Training and Vietnamese Overseas Scholarship Program (VOSP − Project 322) for his Ph.D. grant.

References

[1] M.N. Baibich, J.M. Broto, A. Fert, F. Nguyen van Dau, F. Petroff, P. Etienne, G. Creuzet, A. Friedrich, J. Chazeles, Phys. Rev. Lett. 61 (1988) 2472−2475.
[2] G.A. Prinz, Science 282 (1998) 1660−1663.
[3] F.J. Himpsel, J.E. Ortega, G.J. Mankey, R.F. Willis, Adv. Phys. 47 (4) (1998) 511−597.
[4] S.A. Nikitov, Ph. Tailhades, Opt. Commun. 199 (5−6) (2001) 389−397.

[5] Yu V. Gulyaev, S.A. Nikitov, L.V. Zhivotovskii, A.A. Klimov, Ph. Tailhades, L. Presmanes, C. Bonningue, C.S. Tsai, S.L. Vysotskii, Y.A. Filimonov, JETP Lett. 77 (2003) 567−570.
[6] P. Jiang, J.F. Bertone, K.S. Hwang, V.L. Colvin, Chem. Mater. 11 (1999) 2132−2140.
[7] M. Shinomura, T. Sawadaishi, Curr. Opin. Colloid Interface Sci. 6 (1) (2001) 11−16.
[8] J. Malesko, Mater. Sci. Eng., C 4 (1996) 199−204.
[9] E. Mugnier, I. Pasquet, A. Barnabé, L. Presmanes, C. Bonningue, Ph. Tailhades, Thin Solid Films 493 (2005) 49−53.
[10] V.L. Colvin, MRS Bull. (2001) 637−641.
[11] M.G.M. Miranda, E. Esteves-Rams, G. Martinez, M.N. Baibich, Phys. Rev. B 68 (2003) 01443.
[12] M.G.M. Miranda, A.T. da Rosa, R. Hinrichs, U. Golla-Schindler, A.B. Antunes, G. Martinez, E. Esteves-Rams, M.N. Baibich, Physica B 384 (2006) 175−178.
[13] A. Hutten, D. Sudfeld, K. Wojcrykowski, P. Jutzi, G. Reiss, J. Magn. Magn. Mater. 262 (2003) 23−31.
[14] J. Robin, Ann. Chim. (Paris) 10 (1955) 389−412.
[15] M. Takahashi, M.E. Fine, J. Am. Ceram. Soc. 53 (11) (1970) 633−634.
[16] M. Takahashi, J.R.C. Guimares, M.E. Fine, J. Am. Ceram. Soc. 54 (6) (1971) 291−295.
[17] S. Hirano, T. Yogo, K. Kikuta, E. Asai, K. Sugiyama, H. Yamamoto, J. Am. Ceram. Soc. 76 (7) (1993) 1788−1792.
[18] I.H. Jung, S. Decterov, A.D. Pelton, H.M. Kim, Y.B. Kang, Acta Mater. 52 (2004) 507−519.
[19] A. Rousset, P. Mollard, C. Bonino, M. Gougeon, Ph. Tailhades, European Patent, EP 86 905.853.7., 1986.
[20] J. Rodriguez-Carvajal, Abstracts of the Satellite Meeting on Powder Diffraction of the XV Congress of the IUCr, vol. 127, Toulouse, France, 1990.
[21] Ph. Tailhades, C. Villette, A. Rousset, G.U. Kulkarni, K.R. Kannan, C.N.R. Rao, M. Lenglet, J. Solid State Chem. 141 (1) (1998) 56−63.
[22] I. Chassaing, L. Presmanes, Ph. Tailhades, A. Rousset, Solid State Ionics 58 (3−4) (1992) 261−267.
[23] P.J. Murray, J.W. Linnett, J. Phys. Chem. Solids 37 (1976) 1041−1042.
[24] S. Kawano, N. Achiwa, Mater. Res. Bull. 11 (1976) 911−916.
[25] J.W.D. Martens, W.L. Peeters, H.M. Van Noort, J. Phys. Chem. Solids 46 (1985) 411−416.
[26] P. Poix, Bull. Soc. Chim. Fr. 2 (1965) 1085−1087.
[27] R.J. Harrison, A. Putnis, Surv. Geophys. 19 (1999) 461−520.
[28] P.B. Hirsch, A. Howie, R.B. Nicholson, D.W. Pashley, M.J. Whelan, Electron Microscopy of Thin Crystals, Butterworths, London, 1965.